ELSEVIER

International Journal of Heat and Fluid Flow 23 (2002) 769–775

International Journal of HEAT AND FLUID FLOW

www.elsevier.com/locate/ijhff

A proposed mechanism for hydrodynamically-controlled onset of significant void in microtubes

R.C. Chedester, S.M. Ghiaasiaan *

G.W. Woodruff School of Mechanical Engineering, Georgia Institute of Technology, Atlanta, GA 30332-0405, USA

Received 17 July 2001; accepted 7 October 2001

Abstract

Data and analysis have shown that bubble nucleation and ebullition phenomena in microchannels are different than in large channels. The macroscale models and correlations often fail to predict data representing bubble ebullition processes in microchannels. It is hypothesized here that hydrodynamically-controlled onset of significant void in microchannels is due to bubble departure from wall cavities, and the latter process may be controlled by thermocapillary and aerodynamic forces that act on the bubble. Accordingly, the limited available relevant experimental data are semi-analytically modeled, and the soundness of the proposed hypothesis is shown.

Keywords: Microchannels; Onset of significant void; Subcooled boiling; Bubble departure; Thermocapillary; Turbulence

1. Introduction

Microchannels with hydraulic diameters on the order of 0.1–1 mm have important current and potential applications and their thermal-hydraulic characteristics have been studied rather extensively (Mikol, 1963; Acosta et al., 1985; Tong et al., 1997; Yu et al., 1995; Adams et al., 1997; Adams et al., 1999; Peng and Wang, 1993, 1994; Peng et al., 1995; Ghiaasiaan and Laker, 2001; Ghiaasiaan and Abdel-Khalik, 2001). For single-phase flow important differences with large channels have been reported, in particular with respect to turbulent flow, where most of the published data appear to disagree with well-established macroscale correlations. Measured *Nu* values representing turbulent liquid flow in rectangular channels have been consistently lower than those predicted by macroscale correlations (Peng et al., 1995; Wang and Peng, 1994; Peng and Peterson, 1995), while an opposite trend has been observed for turbulent flow in circular microtubes (Yu et al., 1995; Adams et al., 1997; Adams et al., 1999).

Available data dealing with boiling and two-phase flow also suggest important differences between microchannels (defined here as channels for which $D/\lambda \leqslant 0.3$) and commonly applied large channels (Ghiaasiaan and Abdel-Khalik, 2001). In subcooled boiling, the velocity and temperature gradients near the walls of microchannels can be very large, and bubbles resulting from subcooled or saturated boiling can be extremely small (Vandervort et al., 1992; Wang and Peng, 1994). The occurrence of extremely small bubbles significantly impacts the various subcooled boiling processes including the onset of nucleate boiling (ONB), onset of significant void (OSV) (Kennedy et al., 2000), and departure from nucleate boiling (Celata et al., 1993). Recently, Ghiaasiaan and Chedester (in press) hypothesized that the occurrence of ONB in microchannels depends on the relative magnitudes of the thermocapillary force, that tends to suppress the bubbles, and the aerodynamic force, that tends to lift the bubbles, and they developed a semi-empirical method for the prediction of ONB conditions in microtubes.

The objective of this paper is to show that a similar hypothesis may be applicable to the hydrodynamically-controlled OSV process in microtubes. The outline of the remainder of this paper is as follows. The method used for the prediction of near-wall velocity and temperature

* Corresponding author. Tel.: +1-404-894-3746; fax: +1-404-894-8496.

E-mail address: seyed.ghiaasiaan@me.gatech.edu (S.M. Ghiaasiaan).

0142-727X/02/$ - see front matter © 2002 Published by Elsevier Science Inc.
PII: S0142-727X(02)00199-6

Nomenclature

A, B, C	empirical coefficients
c_p	specific heat (J/kg K)
D	channel diameter (m)
f	D'Arcy friction factor
F_A	aerodynamic force (N)
F_σ	thermocapillary force (N)
G	mass flux (kg/m^{2}s)
h	convection heat transfer coefficient (W/m K)
h_{fg}	latent heat of vaporization (J/kg)
k	thermal conductivity (W/m K)
l	length scale defined in Eq. (20)
Nu	Nusselt number $= hD/k_L$
P	pressure (Pa)
Pe	Peclet number $= \overline{U}D/\alpha_L$
Pr	Prandtl number $= \nu_L/\alpha_L$
q''	heat flux (W/m^2)
r	radial coordinate (m)
R	channel radius (m)
R_B^*	dimensionless bubble radius defined in Eq. (19)
Re	Reynolds number $= \overline{U}D/\nu_L$
T	temperature (K)
u	velocity (m/s)
$\overline{U}$	channel average velocity (m/s)
u^*	friction velocity $= \sqrt{\tau_w/\rho_L}$(m/s)
v	specific volume (m^3/kg)
u^+	dimensionless velocity $= u/u^*$
y	distance from the wall (m)
y_B	height of bubble tip above the wall surface (m)
y^+	dimensionless distance from wall $= yu^*/\nu_L$
y_n^+	parameter in Reichardt's eddy diffusivity model

Greeks

α	thermal diffusivity (m^2/s)
γ	dimensionless parameter defined in Eq. (18)
ε_H	heat transfer eddy diffusivity (m^2/s)
ε_M	momentum eddy diffusivity (m^2/s)
κ	Karman's constant
λ	Laplace length scale $= \sqrt{\sigma/g(\rho_L - \rho_g)}$ (m)
μ	dynamic viscosity (kg/m s)
ν	kinematic viscosity (m^2/s)
θ	azimuthal angle (R)
θ_0	contact angle (R)
ρ	density (kg/m^3)
σ	surface tension (N/m)
τ	shear stress (Pa)

Subscripts

B	bubble
b	bulk
exp	experiment
f	saturated liquid
g	saturated vapor, gas
L	liquid
mod	model
sat	saturation
w	wall
0	constant property

Superscripts

−	average
+	in wall units

Acronyms

OFI	onset of flow instability
ONB	onset of nucleate boiling
OSV	onset of significant void

profiles in turbulent microtube flow is first described, followed by a brief discussion of OSV and onset of flow instability (OFI) phenomena. A semi-empirical model for OSV that is based on the above-mentioned hypothesis is then described and is followed by concluding remarks.

2. Fully-turbulent flow in a microtube

Turbulent characteristics of liquid flow in microtubes may be different than large tubes (Ghiaasiaan and Laker, 2001). The turbulent velocity and temperature profiles, which affect wall heat transfer and thereby the bubble nucleation process, are therefore also likely to be different for microchannels.

For incompressible, fully-developed and constant property flow in a circular tube it can be easily shown that:

$$Re = \frac{\overline{U}D}{\nu_L} = 4\int_0^{R^+} u^+ \,\mathrm{d}y^+ - \frac{4}{R^+}\int_0^{R^+} u^+ y^+ \,\mathrm{d}y^+ \tag{1}$$

where $y^+ = yu^*/\nu_L$; $u^+ = u/u^*$; and

$$u^* = \sqrt{\tau_w/\rho_L} = \overline{U}\sqrt{f/8} = 2R^+\overline{U}/Re \tag{2}$$

For smooth, circular tubes the fully-developed turbulent velocity profile obeys the well-known law of the wall distribution with $\kappa = 0.4$ and $B = 5.5$ (Schlichting, 1968; Von Karman, 1939). Surface roughness and particles, furthermore, modify the velocity profile. The channel friction factor and convection heat transfer coefficient

depend on the turbulent velocity profile according to (Petukhov, 1970):

$$f = \frac{8R^{+4}}{Re}\left\{\int_0^{R^+}\left[\int_{r^+}^{R^+}\frac{r^+}{1+\varepsilon_M/\nu_L}\,dr^+\right]r^+\,dr^+\right\}^{-1} \tag{3}$$

$$\frac{k_L}{hD} = \frac{1}{Nu} = \frac{2}{(\overline{U}^+R^{+2})^2}\int_0^{R^+}\left\{\left(\int_0^{r^+}u^+r^+\,dr^+\right)^2 \times\left[\left(1+\left(\frac{\varepsilon_H}{\varepsilon_M}\right)\mathrm{Pr}\frac{\varepsilon_M}{\nu_L}\right)r^+\right]^{-1}\right\}dr^+ \tag{4}$$

where

$$u^+ = \frac{1}{R^+}\int_{r^+}^{R^+}\frac{r^+\,dr^+}{1+\varepsilon_M/\nu_L} \tag{5}$$

Using the above equations along with an appropriate eddy diffusivity model, the velocity profile and heat transfer coefficient in the channel can be calculated. The dimensionless temperature profile can also be expressed as (Petukhov, 1970):

$$T^+ = \frac{\rho_f c_{pf}u^*}{q''_w}(T_w - T_L) = \frac{2Pr}{\overline{U}^+R^+}\int_{r^+}^{R^+}\left\{\left(\int_0^{r^+}u^+r^+\,dr^+\right) \times\left[r^+\left(1+\left(\frac{\varepsilon_H}{\varepsilon_M}\right)Pr\frac{\varepsilon_M}{\nu_L}\right)\right]^{-1}\right\}dr^+ \tag{6}$$

A well-proven expression for eddy diffusivity in tubes is (Reichardt, 1951):

$$\varepsilon_M/\nu_L = \kappa\lfloor y^+ - y_n^+\tanh(y^+/y_n^+)\rfloor \tag{7}$$

for $y^+ \leqslant 50$, and

$$\varepsilon_M/\nu_L = (\kappa/3)y^+\lfloor 0.5 + (r^+/R^+)^2\rfloor(1+r^+/R^+) \tag{8}$$

for $y^+ > 50$, where $\kappa = 0.4$ and $y_n^+ = 11$.

The above equations were used for the calculation and correlation of the wall heat transfer coefficient and friction factor by Petukhov (1970), who also showed that the effect of the liquid property variations with temperature can be accounted for by writing:

$$(Nu/Nu_0) = (\overline{\mu}/\mu_w)^{0.11} \tag{9}$$

$$(f/f_0) = (7-\overline{\mu}/\mu_w)/6 \tag{10}$$

Ghiaasiaan and Laker (2001) showed that the forced-convection heat transfer data of Adams et al. (1997, 1999), for $Re \leqslant 20\,000$, could be well-predicted by the above equations provided that the parameters in the Reichardt eddy diffusivity model (Reichardt, 1951) are modified as follows: $\kappa = 0.47$–0.5 while $y_n^+ = 11$ (equivalent to a stronger turbulent energy transport in the pipe turbulent core, in comparison with large tubes); or $y_n^+ = 8$–9 while $\kappa = 0.4$ (equivalent to stronger damping in the near-wall zone).

3. Onset of significant void and onset of flow instability in microchannels

In subcooled flow boiling, the OSV point represents the point downstream of which bubbles that detach from the wall and mix with the subcooled liquid core can survive condensation, and lead to a rapid increase in the generation of void fraction. In macroscale experiments the OSV point can be easily identified by measuring the axial void fraction profile, and defining the OSV as the point downstream of which the slope of the void fraction profile is significant (Staub, 1968; Rogers et al., 1987; Bibeau and Salcudeau, 1994a,b). This technique cannot be easily applied to microchannels, and instead the heated channel pressure drop-mass flux (ΔP–G) characteristic curve can be used for the estimation of the OSV points (Roach et al., 1999; Kennedy et al., 2000; Inasaka et al., 1989); a method that has also been applied to large channels in the past (Johnston, 1989).

The general form of the ΔP–G curve, obtained by measuring the total pressure drop across a test section subject to a constant thermal load and a variable subcooled coolant mass flux with invariant inlet temperature under low and moderate system pressures, is depicted in Fig. 1 (Yadigaroglu, 1981). The OFI point is defined as the relative minimum point on the curve, and is a crucial operational threshold for boiling systems. Since OSV occurs at a flow rate only slightly higher than OFI (or at a slightly lower heat flux than OFI in tests where heat flux is varied while the mass flux is maintained constant), the conditions leading to OFI can be used for estimating the OSV conditions. Inasaka et al. (1989) measured the OFI parameters in heated cylindrical test sections with

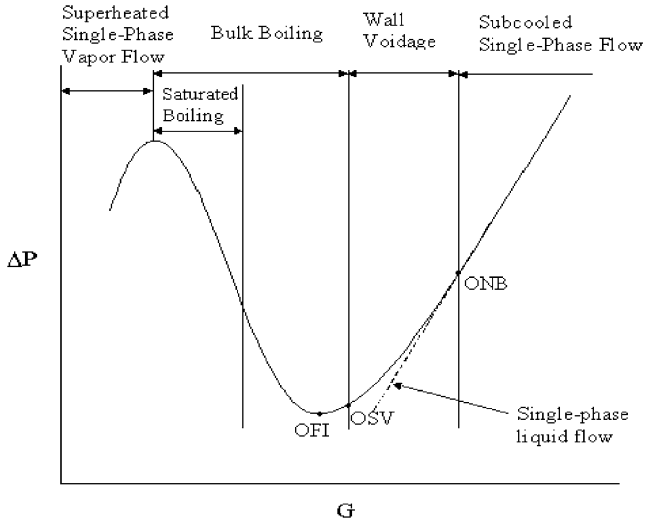

Fig. 1. Pressure drop–mass flux characteristic curve for a uniformly-heated channel.

1 and 3 mm inner diameters, using subcooled water with $G = 7000$–$20\,000$ kg/m^2 s. Most of the data of the latter authors represent hydrodynamically-controlled OSV, and their data representing their 1 mm-diameter test section were utilized in this study. Roach (1999), Kennedy et al. (2000), and Blasick et al. (2000) have performed extensive experiments dealing with low flow rate OFI in microchannels and thin annuli. Their data, however, are all in the low *Pe* range, and represent thermally-controlled OSV.

4. Modeling the hydrodynamically-controlled OSV

Widely-used models for OSV can be divided into two groups: the empirical correlations that address low mass flux (thermally-controlled) as well as high mass flux (hydrodynamically controlled) OSV (Saha and Zuber, 1974; Ünal, 1975); and mechanistic bubble-departure models that primarily apply to hydrodynamically-controlled OSV (Levy, 1967; Staub, 1968; Rogers et al., 1987). The latter models all assume that OSV occurs when forces tending to slide the bubbles formed on the wall crevices overcome the resistance posed by surface tension. Careful visual observations in more recent experimental studies (Bibeau and Salcudeau, 1994a,b) have shown that bubble ejection normal to the wall, rather than bubble detachment and motion parallel to the wall, may actually be primarily responsible for OSV, at least for low pressure water and low liquid velocities. In microchannels, furthermore, due to the occurrence of very large temperature and velocity gradients near the heated walls, the relative magnitudes of forces that act on bubbles are different than in large systems, implying that the phenomenology of bubble ebullition in microchannels may be different than large systems. Better, experimentally-based understanding of the bubble ebullition process in microchannels is evidently needed before rigorous phenomenological models can be developed. In view of the unavailability of relevant experimental data, therefore, a simple phenomenological model that can be supported and justified by physical arguments will be developed.

We assume that a bubble near departure is a deformed, chopped spheroid, as depicted in Fig. 2 (Rogers et al., 1987), and is subject to aerodynamic, drag and surface tension forces. The departing bubble at the OSV point is assumed to be surrounded by liquid warmer than itself just up to its tip (Hsu, 1962; Levy, 1967), therefore:

$$T_B = T_L(y_B) \tag{11}$$

where, from the Clausius–Clapeyron relation:

$$T_B = T_{sat}(P)\left[1 + \frac{2\sigma}{R_B}\frac{\rho_f - \rho_g}{\rho_f \rho_g h_{fg}}\right] \tag{12}$$

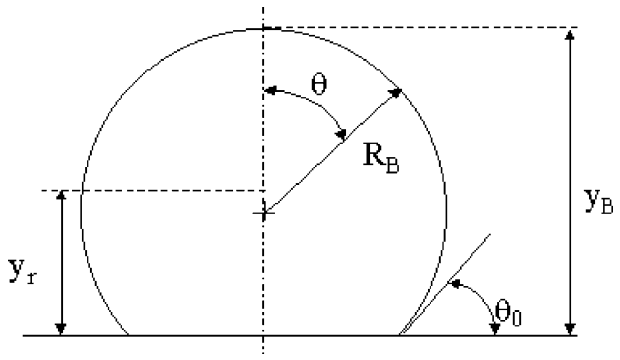

Fig. 2. Idealized bubble configuration at departure.

where

$$y_B = 2y_r = R_B(1 + \cos\theta_0) \tag{13}$$

A multitude of forces act on heterogeneously-generated bubbles, and semi-empirical expressions for the prediction of the magnitude of these forces have been developed for heterogeneous bubbles that occur during fully-developed nucleate boiling in macroscale systems (Klausner et al., 1993; Zeng et al., 1993). The applicability of these expressions to the bubble ebullition processes in microchannels is questionable, however.

It is hypothesized here that bubble departure at the OSV point in microchannels occurs when, in addition to Eq. (11) being satisfied, the aerodynamic force on a bubble overcomes the thermocapillary force (the force resulting from the non-uniformity of surface tension over the bubble surface, itself resulting from non-uniformity of the interfacial temperature), which tends to resist bubble detachment. For the chopped-spherical bubble in Fig. 2, assuming that the bubble size is negligibly small in comparison with the channel radius, and assuming that the liquid-side thermal resistances are negligible in comparison with the resistances associated with the bubble interior and bubble–liquid interface, the upper limit of the thermocapillary force can be represented as:

$$F_\sigma = 2\pi R_B^2 \int_0^{\pi-\theta_0} [(\partial\sigma/\partial T_L)(\partial T_L/\partial y)]_{y_\theta} \sin^2\theta \, d\theta \tag{14}$$

where

$$y_\theta = y_B - R_B(1 - \cos\theta) \tag{15}$$

The bubble, however, would distort its surrounding flow field and is unlikely to support the aforementioned complete thermal nonequilibrium at its surface. Rigorous modeling of thermocapillary and aerodynamic forces is thus difficult. An estimate of the relative magnitudes of the thermocapillary and aerodynamic forces, however, can be obtained by noting that:

$$F_\sigma \sim R_B(\sigma_f - \sigma_w) \tag{16}$$

$$F_A \sim R_B^2 \rho_L U_r^2 \tag{17}$$

where U_r represents the undisturbed liquid velocity at y_r, and is obtained from the turbulent velocity profile, and σ_f and σ_w are the surface tension values calculated at T_{sat} and T_w, respectively. The ratio of the orders-of-magnitude of the thermocapillary and aerodynamic forces can thus be represented by the dimensionless parameter γ, defined as:

$$\gamma = \frac{\sigma_f - \sigma_w}{\rho_L U_r^2 R_B} \tag{18}$$

The radius of the bubbles departing from the wall at OSV should thus be expected to depend on γ and Pe.

Fig. 3 displays the values of R_B^*, defined in the following equations, based on the experimental OFI data of Inasaka et al. (1989) for their 1 mm-diameter test section:

$$R_B^* = R_B/l \tag{19}$$

$$l = \rho_L v_L^2/\sigma \tag{20}$$

where σ, used in the definition of the length scale l, represents the temperature $(T_w + \overline{T}_L)/2$. The latter length scale can be derived based on a dimensional analysis using liquid properties, but excluding gravity, and is consistent with the way a dimensionless surface tension parameter is defined when a strong dependence of the latter parameter on the velocity or rate of shear is avoided. Dividing l by a relevant geometric length (e.g., R) results in the definition of a surface tension parameter which does not depend on velocity (Preziosi et al., 1989). Although hydrodynamically-controlled conditions ($Pe \leqslant 7 \times 10^4$ in large systems (Saha and Zuber, 1974)) are of interest here, data representing $Pe \cong 4 \times 10^4$ have also been included in the figure. The depicted values of R_B^* in Fig. 3 were calculated as follows. Knowing the test conditions for each OFI data point (assumed to approximately represent the OSV point), the microchannel velocity and temperature profiles were obtained using Eqs. (1)–(8) while following the procedure detailed in Ghiaasiaan and Laker (2001). These numerical calculations were performed by using a total of 1800 radial nodes, with 1000 equal-sized nodes representing the $1 < r/R \leqslant 0.85$ region of the tube cross-section, and another 800 equal-sized radial nodes for the remainder of the cross-section. The standard values of $\kappa = 0.4$ and $y_n^+ = 11$ were used for these calculations everywhere unless otherwise stated. The bubble radius that satisfied Eq. (11) at the OSV point was then calculated, followed by the calculation of R_B^* from Eq. (19).

Fig. 3 shows a clear dependence of R_B^* on both γ and Pe, consistent with the aforementioned hypothesis regarding the crucial role of the thermocapillary force. In fact, the data points in Fig. 3 can be represented by the following simple correlation:

$$R_B^* = C e^{APe} \gamma^B \tag{21}$$

where:

$$A = -1.49 \times 10^{-5}$$
$$B = -0.63$$
$$C = 2200$$

The predictions of the present OSV model are now compared with the OFI data of Inasaka et al. (1989) in Fig. 4, where data with $Pe \geqslant 7.5 \times 10^4$ (which are considered to be hydrodynamically-controlled) are used. The mean and standard deviation of the statistic $(1 - q''_{OSV}/q''_{OSV,exp})$ are 0.144 and 0.193, respectively. The range of the important dimensionless parameters in the data are:

$$75\,000 \leqslant Pe \leqslant 125\,000$$
$$35\,000 \leqslant Re_L \leqslant 70\,000$$
$$0.004 < \gamma < 0.4$$
$$65\,000 < R/l < 335\,000$$

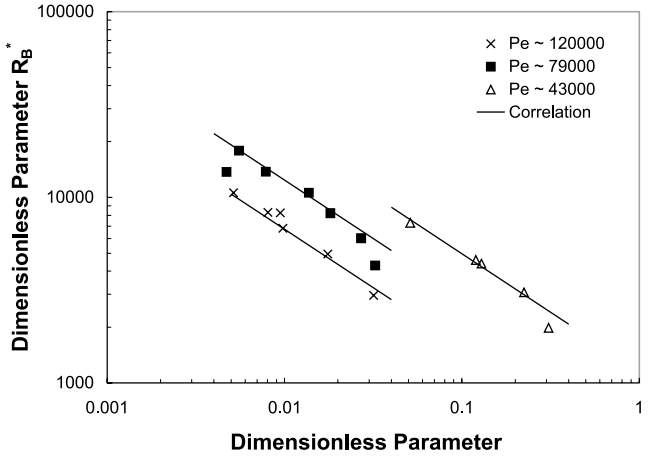

Fig. 3. Calculated values of dimensionless bubble radii for the data of Inasaka et al. (1989), for $\kappa = 0.4$, $y_n^+ = 11$.

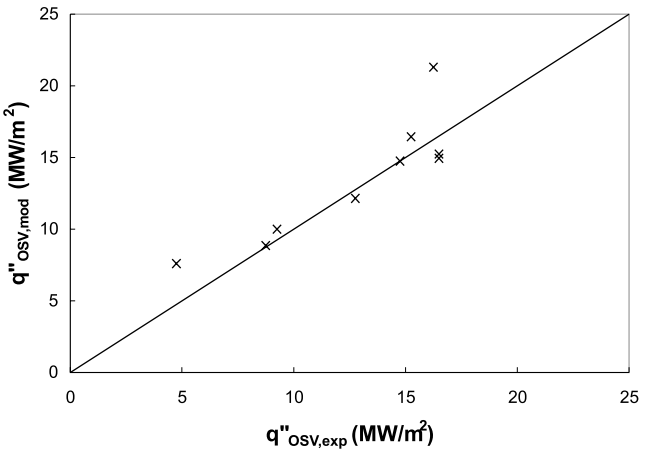

Fig. 4. Comparison between the predicted q''_{OSV} values with the q''_{OFI} values in the experiments of Inasaka et al. (1989), for $\sigma = 0.4$, $y_n^+ = 11$.

The model calculations depicted in Fig. 4 were performed as follows. Knowing the local mean subcooled water conditions, the wall heat flux, q'', was iteratively changed, using the repeated bisections method, for solving the equations involved in the problem. For any q'' , first the coolant temperature distribution was obtained. Using the coolant temperature profile, the radial location where Eqs. (12,13,21) were all satisfied was found. Eq. (11) was then used as the requirement for convergence in the iterations. Convergence was easily achieved for all data points and parametric tests for which the hydrodynamically-controlled assumption was valid, with only a few exceptions. For cases involving highly subcooled water ($T_{sat} - \overline{T}_L > 25$ °C) numerical convergence did not happen and Eq. (11) could not be satisfied exactly. This is likely due to the limited range and the particular mathematical form of Eq. (21), and may not be considered as proof contrary to the proposed underlying hypothesis.

It is emphasized here that the above hypothesis and calculations are not applicable to large channels where typically the parameter R_B^* is very large, and Eq. (21) can never be satisfied.

The above calculations, as noted earlier, were based on assuming $\kappa = 0.4$ and $y_n^+ = 11$ for the eddy diffusivity model of Reichardt (1951). However, it was recently noted that the available data dealing with turbulent forced convection in circular microtubes could be explained by the modification of the well-known eddy diffusivity profiles originally developed for macroscale pipe flow (Ghiaasiaan and Laker, 2001). The calculations described above were repeated in order to examine the sensitivity of the results to microtube turbulent characteristics. Fig. 5 is similar to Fig. 3 and was obtained by assuming $\kappa = 0.4$ and $y_n^+ = 8.5$; the latter values of κ and y_n^+ have been found to well-predict some recent microtube single-phase liquid heat transfer data (Ghiaasiaan and Laker, 2001). The systematic and obvious dependence of R_B^* on Pe and γ is evidently maintained with the modified microchannel eddy diffusivity profile. With these eddy diffusivity profile parameters, however, the constants in Eq. (21) have to be replaced with:

$$A = -1.52 \times 10^{-5}$$

$$B = -0.6$$

$$C = 2100$$

A similar set of calculations with $\kappa = 0.48$ and $y_n^+ = 11$ (Ghiaasiaan and Laker, 2001) lead to the following values for the constants in Eq. (21):

$$A = -1.43 \times 10^{-5}$$

$$B = -0.6$$

$$C = 1975$$

The relative sensitivity of the results to the microtube turbulence characteristics confirms the need for more careful investigation of turbulence in microchannels. It is also emphasized that the data used as the basis for the validation of the main hypothesis suggested in this paper, and the development of the resulting correlations, were limited in scope. More experimental studies are evidently needed.

Some parametric calculation results for a 1 mm-diameter heated channel, with subcooled water as the coolant, are displayed in Fig. 6, where the predictions of the present model are depicted. The predictions of the correlation of Saha and Zuber (1974) are also shown for comparison purposes, and for better depiction of the trends. These calculations are limited to water at 2.5 bar pressure, consistent with the data used as the basis for the derivation of Eq. (21). The proposed hypothesis and the resulting empirical correlation correctly predict the major known and expected trends: the OSV heat flux monotonically increases with increasing mean liquid velocity and subcooling, and within the depicted parameter range it is systematically underpredicted by the macroscale correlation of Saha and Zuber (1974).

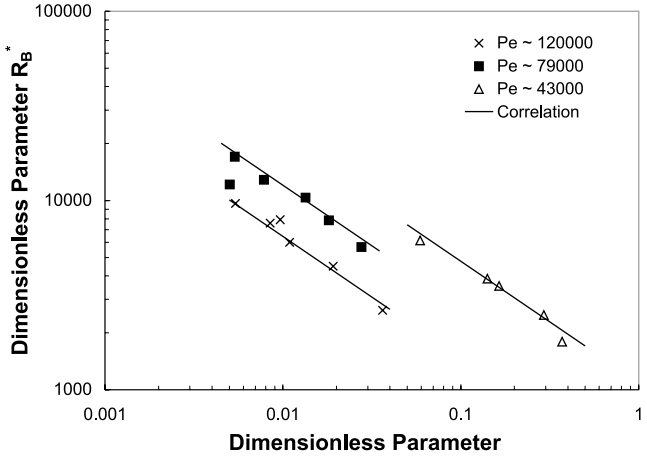

Fig. 5. Calculated values of dimensionless bubble radii for the data of Inasaka et al. (1989), for $\kappa = 0.4$, $y_n^+ = 8.5$.

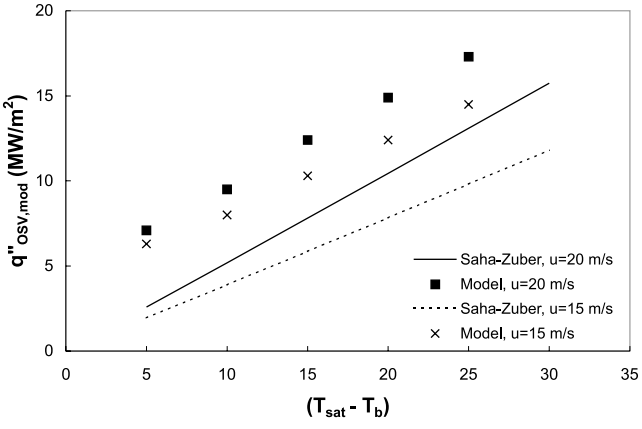

Fig. 6. Model-predicted q''_{OSV} for subcooled water flow in a 1 mm-diameter circular channel ($P = 2.5$ bar): parametric effects of coolant velocity and subcooling.

5. Concluding remarks

The hydrodynamically-controlled OSV in heated microtubes was addressed in this paper. It was hypothesized that the thermocapillary and aerodynamic forces that act on bubbles forming on the wall cavities may control the occurrence of OSV in microtubes. The soundness of the proposed hypothesis was shown by deriving a simple semi-empirical correlation for the radius of departing bubbles at the OSV point based on the OFI data of Inasaka et al. (1989). The effect of microtube turbulence characteristics on the model parameters was also examined.

While the results are believed to support the proposed hypothesis and the soundness of the applied modeling methodology, the limited scope of the available relevant experimental data is noted, and the need for more experimental studies is emphasized.

References

Acosta, R., Muller, R., Tobins, C., 1985. Transport processes in narrow (capillary) channels. AIChE J. 31, 473–482.

Adams, T.A., Abdel-Khalik, S.I., Jeter, S.M., Qureshi, Z., 1997. An experimental investigation of single-phase forced convection in microchannels. Int. J. Heat Mass Transfer 41, 851–859.

Adams, T.M., Ghiaasiaan, S.M., Abdel-Khalik, S.I., 1999. Enhancement of liquid forced convection heat transfer in microchannels due to the release of dissolved noncondensables. Int. J. Heat Mass Transfer 42, 3563–3573.

Bibeau, E.L., Salcudeau, M., 1994a. Subcooled void growth mechanisms and prediction at low pressure and low velocity. Int. J. Multiphase Flow 20, 837–863.

Bibeau, E.L., Salcudeau, M., 1994b. A study of bubble ebullition in forced-convective subcooled nucleate boiling at low pressure. Int. J. Heat Mass Transfer 37, 2245–2259.

Blasick, A.M., Dowling, M.F., Abdel-Khalik, S.I., Ghiaasiaan, S.M., Jeter, S.M., 2000. The onset of flow instability in uniformly heated horizontal narrow annuli. 8th Int. Conf. Nucl. Eng. (ICONE–8), Baltimore, Maryland, April 2–6.

Celata, G.P., Cumo, M., Mariani, A., Nariai, H., Inasaka, F., 1993. Influence of channel diameter on subcooled flow boiling burnout at high heat fluxes. Int. J. Heat Mass Transfer 44, 3407–3409.

Ghiaasiaan, S.M., Abdel-Khalik, S.I., 2001. Two-phase flow in microchannels. Progress in Heat Transfer 34, 145–254.

Ghiaasiaan, S.M., Chedester, R.C. Boiling incipience in microchannels. Int. J. Heat Transfer, in press.

Ghiaasiaan, S.M., Laker, T.S., 2001. Turbulent forced convection in microtubes. Int. J. Heat Mass Transfer 44, 2777–2782.

Hsu, Y.Y., 1962. On the size range of active nucleation cavities on a heating surface. J. Heat Transfer 84C, 207–216.

Inasaka, F., Nariai, H., Shimura, T., 1989. Pressure drop in subcooled boiling in narrow tubes. Heat Transfer-Jpn. Res. 18, 70–82.

Johnston, B.S., 1989. Subcooled boiling of downward flow in a vertical annulus. ASME HTD 109, 149–156.

Kennedy, J.E., Roach Jr, G.M., Dowling, M.E., Abdel-Khalik, S.I., Qureshi, Z.H., 2000. The onset of flow instability in uniformly heated horizontal microchannels. J. Heat Transfer 122, 118–125.

Klausner, J.F., Mei, R., Bernhard, D.M., Zeng, L.Z., 1993. Vapor bubble departure in forced convection boiling. Int. J. Heat Mass Transfer 36, 651–662.

Levy, S., 1967. Forced convection subcooled boiling: prediction of vapor volumetric fraction. Int. J. Heat Mass Transfer 28, 1116–1129.

Mikol, E.P., 1963. Adiabatic single and two-phase flow in small bore tubes. ASHRAE J. 5, 75–86.

Peng, X.F., Peterson, G.P., 1995. The effect of thermofluid and geometrical parameters on convection of liquids through rectangular microchannels. Int. J. Heat Mass Transfer 38, 755–758.

Peng, X.F., Wang, B.-X., 1993. Forced convection and flow boiling heat transfer for liquid flowing through microchannels. Int. J. Heat Mass Transfer 36, 3421–3427.

Peng, X.F., Wang, B.-X., 1994. Liquid flow and heat transfer in microchannels with and without phase change. Proc. 10th Int. Heat Transfer Conference 1, pp. 159–177.

Peng, X.F., Wang, B.-X., Peterson, G.P., Ma, H.P., 1995. Experimental investigation of heat transfer in flat plates with rectangular microchannels. Int. J. Heat Mass Transfer 38, 127–137.

Petukhov, B.S., 1970. Heat transfer and friction in turbulent pipe flow with variable physical Properties. Adv. Heat Transfer 6, 503–565.

Preziosi, L., Chen, K., Joseph, D., 1989. Lubricated pipelining: stability of core-annular flow. J Fluid Mech. 201, 323–356.

Reichardt, H., 1951. Die grundlagen des turbulent warmeuberganges. Arch. Ges. Warmetech 2, 129–142.

Roach Jr., G.M, Abdel-Khalik, S.I., Ghiaasiaan, S.M., Jeter, S.M., 1999. Low flow onset of flow instability in heated microchannels. Nucl. Sci. Eng. 133, 106–117.

Rogers, J.T., Salcudean, M., Abdullah, Z., McLeod, D., Poirer, D., 1987. The onset of significant void in up-flow boiling of water at low pressures and velocities. Int. J. Heat Mass Transfer 30, 2247–2260.

Saha, P., Zuber, N., 1974. Point of net vapor generation and vapor void fraction in subcooled boiling. Proc. 5th Int. Heat Transfer Conference, Tokyo, Japan, pp. 175–179.

Schlichting, H., 1968. Boundary-Layer Theory. McGraw-Hill, New York.

Staub, F.W., 1968. The void fraction in subcooled boiling: prediction of the initial point of net vapor generation. J. Heat Transfer 90, 151–157.

Tong, W., Bergles, A.E., Jensen, M.K., 1997. Pressure drop with highly subcooled flow boiling in small-diameter tubes. Exp. Thermal Fluid Sci. 15, 202–212.

Ünal, H.C., 1975. Determination of the initial point of net vapor generation in flow boiling systems. Int. J. Heat Mass Transfer 18, 1095–1099.

Vandervort, C.L., Bergles, A.E., Jensen, M.K., 1992. Heat transfer mechanisms in very high heat flux subcooled boiling. ASME Fundamentals Subcooled Flow Boiling, 1–9.

von Karman, T., 1939. The analogy between fluid friction and heat transfer. Trans. ASME, 705.

Wang, B.-X., Peng, X.F., 1994. Experimental investigation of liquid forced-convection heat transfer through microchannels. Int. J. Heat Mass Transfer 37, 73–82.

Yadigaroglu, G., 1981. In: Two-phase flow instabilities and propagation phenomena, in thermohydraulics of two-phase systems for industrial design and nuclear engineering. Hemisphere, Washington DC, pp. 353–403.

Yu, W., Warrington, R.O., Barron, R.F., Ameel, T.A., 1995. An experimental and theoretical investigation of fluid flow and heat transfer in microtubes. Proc. ASME/JSME Thermal Eng. Conf. 1, 523–530.

Zeng, L.Z., Klausner, J.F., Mei, R., 1993. A unified model for the prediction of bubble detachment diameters in boiling systems-II. Flow boiling. Int. J. Heat Mass Transfer 36, 2271–2279.